ways denser than the plagioclase on their liquidus, thus precluding crystal settling as the cause for the layering observed in mafic intrusions; and other mechanisms have been invoked [for example, oscillatory nucleation and subsolidus recrystallization (*23*)]. Before this work, the uncertainty in $\bar{V}_{H_2O}$ precluded a quantitative evaluation of the effect of dissolved water on the density of the iron-rich liquids, which can now be calculated.

Estimates of pre-eruptive water contents in tholeiitic basalts [up to 1 weight % H_2O (*24*)] are derived primarily from analyses on glasses from mid-ocean ridges and hot spots. Because H_2O is incompatible in the anhydrous phenocryst assemblage of tholeiitic basalts, crystallization causes both FeO^T and H_2O to increase in residual liquids. At a FeO^T concentration of 15.8 weight % [the peak value observed in an experimental tholeiitic liquid at the point of Fe-Ti oxide saturation (*25*)], only ~0.8 weight % dissolved water is required to render the liquid less dense than the coexisting plagioclase phenocrysts of An_{58} composition [2.699 g/cm^3 (*25*)]. Such a modest water content could arise after 40% crystallization of a tholeiitic basalt with an initial water content of 0.5 weight % H_2O.

The effect of water on the density of magmatic liquids also relates to models of convection within chambers, driven by thermal and compositional density gradients (*26*). The role of water in offsetting the effect of temperature to promote buoyant ascent of evolved melt along sidewall boundary layers was discussed by Shaw (*27*) and further explored by several others (*28*). The results of our study indicate that a gradient of only 0.16 and 0.25 weight % H_2O, respectively, is all that is required to offset the effect on melt density of a 100°C temperature gradient in a rhyolitic and basaltic melt at crustal depths.

References and Notes

1. M. C. Johnson, A. T. Anderson, M. J. Rutherford, *Rev. Mineral.* **30**, 281 (1994).
2. C. W. Burnham and N. F. Davis, *Am. J. Sci.* **270**, 54 (1971).
3. F. A. Ochs and R. A. Lange, *Contrib. Mineral. Petrol.* **129**, 155 (1997).
4. L. A. Silver *et al.*, *ibid.* **104**, 142 (1990).
5. B. O. Mysen, D. Virgo, F. A. Seifert, *Rev. Geophys. Space Phys.* **20**, 353 (1982).
6. R. A. Lange and I. S. E. Carmichael, *Geochim. Cosmochim. Acta* **51**, 2931 (1987).
7. ———, *Contrib. Mineral. Petrol.* **125**, 167 (1996).
8. G. Moore, T. Vennemann, I. S. E. Carmichael, *Am. Mineral.* **83**, 36 (1998).
9. C. T. Moynihan, *Rev. Mineral.* **32**, 1 (1995); J. A. Tangeman, thesis, University of Michigan, Ann Arbor, MI (1998). The value of T_f' is approximated (±20°C) by the onset of the rapid rise in a glass thermal expansion curve during heating.
10. The density is converted to molar volume as follows: $V^{glass}_{298\ K}$ = gram formula weight/$\rho^{glass}_{298\ K}$.
11. Y. Zhang *et al.*, *Geochim. Cosmochim. Acta* **61**, 3089 (1997) was used for calibration of the FTIR measurements of water (±0.7% relative) on rhyolite glasses. The manometry technique of T. W. Vennemann and J. R. O'Neil [*Chem. Geol.* **103**, 227 (1993)] was used to measure water contents in four KCS glasses (H_2O collection ≥150°C); these data (±0.5% relative) were used to calibrate the FTIR measurements on the remaining KCS glasses. The fitted molar absorptivities for the 5300 cm^{-1} ($H_2O^{molecular}$) and the 4540 cm^{-1} (OH) FTIR bands are 5.90 ± 1.19 cm^2/mol and 4.48 ± 1.04 cm^2/mol, respectively. These errors translate to uncertainties of <0.2 weight % H_2O (absolute).
12. A pressure correction per gigapascal of 2.52 (±0.25) % for the rhyolitic glasses and 1.06 (±0.25) % for the KCS glasses was obtained by comparing the difference between the 1-bar and 1-GPa densities of several anhydrous glasses of each composition. Consistent with a similar correction for hydrous albitic glasses (*3*), there is no evidence that the pressure corrections vary with H_2O concentration, within experimental resolution.
13. R. A. Lange, *Geochim. Cosmochim. Acta* **60**, 4989 (1996); *Contrib. Mineral. Petrol.* **130**, 1 (1997).
14. J. Bockris, J. W. Tomlinson, J. L. White, *Faraday Soc. Trans.* **52**, 299 (1956); D. J. Stein, J. F. Stebbins, I. S. E. Carmichael, *J. Am. Ceram. Soc.* **69**, 396 (1986).
15. M. L. Rivers and I. S. E. Carmichael, *J. Geophys. Res.* **92**, 9247 (1987); V. C. Kress, Q. Williams, I. S. E. Carmichael, *Geochim. Cosmochim. Acta* **52**, 288 (1988); V. C. Kress and I. S. E. Carmichael, *Contrib. Mineral. Petrol.* **108**, 82 (1991).
16. The calculations were done with the compilation in (*7*) and that in R. A. Lange and I. S. E. Carmichael, *Rev. Mineral.* **24**, 25 (1990).
17. Propagated uncertainties in $V^{liq}_{T_f}$ are ~1.1%, with the largest contributions to the error arising from the following three terms: (i) the Archimedean measurement of $\rho^{glass}_{298\ K}$ (<0.2%), (ii) the pressure correction to density (~0.25%), and (iii) the error in the gram formula weight (~0.4%) that is primarily derived from the analytical uncertainty in measuring the H_2O concentration. The uncertainty in α^{glass} of ±15% and in T_f, of ±20°C each contribute <0.1% error to values of $V^{liq}_{T_f}$.
18. P. Richet and A. Polian, *Science* **281**, 396 (1998).
19. L. R. Wager and G. M. Brown, *Layered Igneous Rocks* (Oliver & Boyd, Edinburgh, 1968); T. N. Irvine, J. C. O. Andersen, C. K. Brooks, *Geol. Soc. Am. Bull.* **110**, 1398 (1998).
20. I. H. Campbell, *Lithos* **11**, 311 (1978); A. R. McBirney and R. M. Noyes, *J. Petrol.* **20**, 487 (1979).
21. Y. Bottinga and D. Weill, *Am. J. Sci.* **269**, 169 (1970); I. H. Campbell, P. L. Roeder, J. M. Dixon, *Contrib. Mineral. Petrol.* **67**, 369 (1978).
22. D. J. Fornari *et al.*, *J. Geophys. Res.* **88**, 10519 (1983).
23. G. Brandeis and C. Jaupart, in *Origin of Igneous Layering*, I. Parsons, Ed. (Reidel, Boston, 1987), pp. 613–639; A. E. Boudreau and A. R. McBirney, *J. Petrol.* **38**, 1003 (1997).
24. D. W. Muenow *et al.*, *Nature* **343**, 159 (1990); P. J. Wallace and A. T. Anderson, *Bull. Volcanol.* **59**, 327 (1998).
25. D. Snyder, I. S. E. Carmichael, R. A. Wiebe, *Contrib. Mineral. Petrol.* **113**, 73 (1993).
26. R. J. S. Sparks, H. E. Huppert, J. S. Turner, *Philos. Trans. A R. Soc. London* **310**, 511 (1984); J. S. Turner and I. H. Campbell, *Earth Sci. Rev.* **23**, 255 (1986); D. Martin, R. W. Griffiths, I. H. Campbell, *Contrib. Mineral. Petrol.* **96**, 465 (1987).
27. H. R. Shaw, *Carnegie Inst. Wash. Publ.* **634**, 139 (1974).
28. F. Spera, D. A. Yuen, D. V. Kemp, *Nature* **310**, 764 (1984); A. R. McBirney, B. H. Baker, R. H. Nilson, *J. Volcan. Geotherm. Res.* **24**, 1 (1985); A. Trial and F. Spera, *Geol. Soc. Am. Bull.* **102**, 353 (1990).

29. Supported by NSF (grant EAR-9706075). We thank I. Carmichael, E. Essene, D. Snyder, F. Spera, and two anonymous reviewers for their insightful comments.

16 October 1998; accepted 7 December 1998

Convergence of Transforming Growth Factor–β and Vitamin D Signaling Pathways on SMAD Transcriptional Coactivators

Junn Yanagisawa,[1] Yasuo Yanagi,[1] Yoshikazu Masuhiro,[1] Miyuki Suzawa,[1,2] Michiko Watanabe,[1] Kouji Kashiwagi,[1] Takeshi Toriyabe,[1] Masahiro Kawabata,[3] Kohei Miyazono,[3] Shigeaki Kato[1,2]*

Cell proliferation and differentiation are regulated by growth regulatory factors such as transforming growth factor–β (TGF-β) and the liphophilic hormone vitamin D. TGF-β causes activation of SMAD proteins acting as coactivators or transcription factors in the nucleus. Vitamin D controls transcription of target genes through the vitamin D receptor (VDR). Smad3, one of the SMAD proteins downstream in the TGF-β signaling pathway, was found in mammalian cells to act as a coactivator specific for ligand-induced transactivation of VDR by forming a complex with a member of the steroid receptor coactivator–1 protein family in the nucleus. Thus, Smad3 may mediate cross-talk between vitamin D and TGF-β signaling pathways.

Vitamin D receptor (VDR) is a member of the nuclear receptor superfamily, and acts as a ligand-inducible transcriptional factor with coactivators (*1*, *2*) such as the members of the steroid receptor coactivator–1/transcriptional intermediary factor 2 (SRC-1/TIF2) proteinfamily (*3*) and CREB-binding protein (CBP)/p300 (*4*). Cooperative actions of the growth regulatory factor TGF-β and vitamin D (*5*), and the phenotype of VDR knock-out mice (*6*), indicate that there may be cross-talk between the two signaling pathways. We therefore examined ligand-induced transactivation function of VDR and other nuclear receptors in cells stimulated by TGF-β or bone morphogenetic protein (BMP). VDR expression vectors and

chloramphenicol acetyltransferase (CAT) reporter plasmid were transfected into COS-1 cells, and cells were treated with or without 1,25-dihydroxyvitamin D_3 [1,25$(OH)_2D_3$] or TGF-β (*7–10*). The transactivation function of VDR was significantly enhanced by the treatment with TGF-β (Fig. 1A), but not BMP. The constitutively active forms of either TGF-β type I receptor [TβR-I(TD)] or BMP type I receptor [BMPR-IA(QD) or BMPR-IB(QD)] (*11, 12*) were transfected into COS-1 cells with various nuclear receptor expression plasmids and CAT reporter plasmids bearing their respective response elements (*7–9*). TβR-I(TD), but not BMPR-IA(QD) or BMPR-IB(QD), increased the ligand-induced transactivation activity of VDR (Fig. 1A); however, it did not affect the other tested nuclear receptors: estrogen receptor α (ERα), androgen receptor (AR), glucocorticoid receptor (GR), retinoic acid receptor (RAR), and retinoid X receptor (RXR) (*9, 13*). Transactivation function of VDR was, however, suppressed by transfection with the catalytically inactive TGF-β type I receptor [TβR-I(KR)] (Fig. 1A). Similar results were obtained with other cell lines such as HeLa and HOS (*13*). The presence of TGF-β or BMP receptors did not affect the expression of VDR protein as estimated by protein immunoblotting (*6, 13*). Thus, the ligand-induced transactivation function of VDR was enhanced by TGF-β, but not by BMP signals.

The members of the SMAD protein family (Smad1 through Smad8) are signal transducers of the TGF-β–BMP superfamily (*14*). Smad1 and Smad5 transduce signals for BMPs (*15, 16*), and signals for TGF-β are mediated by Smad2 and Smad3 (*17*). Smad4 acts as a common partner for these pathway-specific SMAD proteins (*18*). When TGF-β or BMP receptors are activated by the binding of cognate ligands, pathway-specific SMADs are phosphorylated by the type I receptor serine-threonine kinases. Phosphorylated SMADs form stable complexes with Smad4, and these complexes translocate into the nucleus where they activate transcription as coactivators or DNA-binding transcription factors (*14, 17–19*), though the overexpressed Smad3 and Smad4 are predominantly localized to the nucleus (*20*). We therefore investigated whether SMAD proteins could enhance the transactivation function of VDR. Neither Smad2 nor Smad4 stimulated the transactivation of VDR (Fig. 1B). However, expression of equivalent amounts of Smad3 did enhance the ligand-induced transactivation function of VDR, and Smad4 and TβR-I(TD) only slightly increased the action of Smad3 (Fig. 1B). When smaller amounts of Smad3 were expressed, TβR-I(TD) caused an additional increase in VDR transactivation beyond that induced by Smad3 (*13*). Moreover, a dominant-negative mutant of Smad3 that inhibits phosphorylation of wild-type Smad3 eliminated the enhancement of VDR transactivation function by wild-type Smad3 (*13*). The enhanced transactivation function of VDR by Smad3 was also observed in vitamin D response elements (VDREs) derived from mouse osteopontin (OP) or human osteocalcin (OC) gene promoters (Fig. 1C) (*8*). Smad1, a signal transducer of BMPs, had no effect on the ligand-induced transactivation of VDR (Fig. 1A). Thus, only Smad3 appears to enhance the ligand-induced transactivation function of VDR.

To test whether SMADs might serve as coactivators of VDR, we examined whether Smad3 physically interacts with VDR in vivo. Although no interaction of VDR with Smad2 was detected in the mammalian two-hybrid system (*21*), which detects protein-protein interactions in vivo, the ligand-dependent interaction of VDR with Smad3 was evident when compared to that of VDR with RXR (Fig. 2A). Interaction of Smad3 with VDR was also tested by coimmunoprecipitation (*22*) of Smad3 and VDR from COS-1 cells transfected with full-length VDR [VDR(1-424)] and FLAG-tagged Smad3. VDR was detected in anti-FLAG immunoprecipitate by protein immunoblotting with antibody to VDR. The presence of 1,25$(OH)_2D_3$ enhanced complex formation of Smad3 and VDR and heterodimerization with RXR (Fig. 2B). These findings indicate that VDR and Smad3 interact in vivo in a ligand-dependent manner.

We assessed interaction of a glutathione S-transferase (GST)–VDR fusion protein (*23*) with in vitro–translated Smad3 protein (*24*). The proteins interacted directly in the presence of 1,25$(OH)_2D_3$. A series of truncated Smad3 proteins showed that the NH_2-terminal Mad homology 1 (MH1) region of

[1]Institute of Molecular and Cellular Biosciences, University of Tokyo, Yayoi, Bunkyo-ku, Tokyo 113-0032, Japan. [2]CREST, Japan Science and Technology, 4-1-8 Honcho, Kawaguchi, Saitama 332, Japan. [3]Department of Biochemistry, The Cancer Institute, Tokyo, Japanese Foundation for Cancer Research (JFCR), and Research for the Future Program, Japan Society for the Promotion of Science, 1-37-1 Kami-Ikebukuro, Toshima-ku, Tokyo 170-8455, Japan.

*To whom correspondence should be addressed. E-mail: uskato@hongo.ecc.u-tokyo.ac.jp

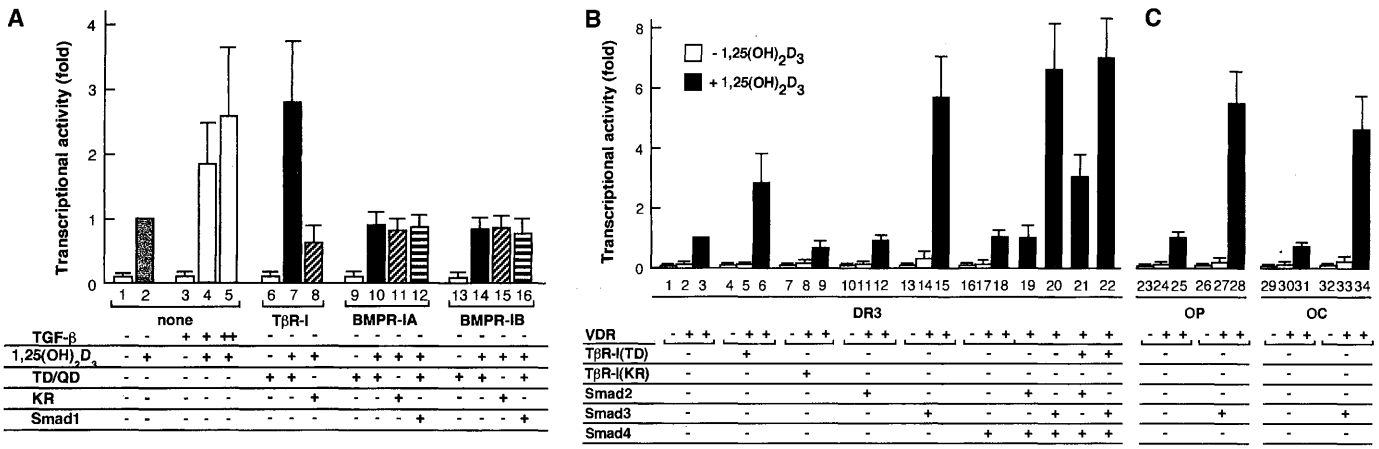

Fig. 1. Enhanced ligand-induced transactivation function of VDR in cells expressing activated TGF-β receptor. (**A**) CAT assays were performed with extracts from the COS-1 cells transfected with VDR expression vector (pSG5-VDR) (1 μg) and CAT reporter plasmid bearing a VDRE (7) (DR3T-G-CAT) (3 μg), together with either constitutively active [TβR-I(TD)] or catalytically inactive [TβR-I(KR)] TGF-β type I receptor expression vector (5 μg), constitutively active [BMPR-IA(QD) and BMPR-IB(QD)] or catalytically inactive [BMPR-IA(KR) and BMPR-IB(KR)] BMP type I receptor expression vectors (5 μg), along with Smad1 expression vector (pcDNA3-Smad1) (5 μg) in the presence (+) or absence (–) of 1,25$(OH)_2D_3$ (10^{-9} M) or TGF-β [0.5 (+) or 1 (++) ng/ml]. (**B**) Increased ligand-induced transactivation function of VDR in cells transfected with Smad3. COS-1 cells were cotransfected with pSG5-VDR (1 μg); either DR3T-G-CAT, OP-G-CAT, or OC-G-CAT (3 μg); either TβR-I(TD) or TbR-I(KR) (5 μg); and Smad2 (pcDNA3-Smad2), Smad3 (pcDNA3-Smad3), or Smad4 (pcDNA3-Smad4) expression vector (5 μg) in the presence or absence of 1,25$(OH)_2D_3$ (10^{-9} M). All values represent averages ± SD of at least three independent experiments.

Smad3 is required for this interaction (Fig. 3A). The MH1 region was also indispensable for the interaction of Smad3 with VDR in the mammalian two-hybrid system with the truncated Smad3 proteins fused to VP16 and GAL4-VDR(DEF) (Fig. 3A). The MH1 region was also required for immunoprecipitation of VDR with Smad3 proteins (Fig. 3B). These results indicated that the MH1 region mediates the interaction of Smad3 with VDR. Smad3 mutants [S3(41-435), S3(68-435), S3(147-435), and S3(238-435)], lacking the VDR interaction domain, did not enhance the ligand-induced transactivation function of VDR, even when the intrinsic transactivation domain (MH2 domain) of Smad3 remained intact (Fig. 3A). In fact, overexpression of such Smad3 mutants suppressed ligand-induced transactivation function of VDR (Fig. 3A).

A series of truncated VDR proteins demonstrated that the middle region of the ligand-binding domain (E domain) of VDR is required for the interaction with Smad3 (Fig. 4A). The COOH-terminal end of VDR is essential for the ligand-induced transactivation function of the VDR ligand-binding domain (AF-2) and directly interacts with the nuclear coactivators in a ligand-dependent way (*25*). The region exhibited no interaction, but rather seemed to have an inhibitory effect on the Smad3 interaction (Fig. 4A). The in vitro binding of Smad3 and VDR was ligand-independent, and the binding was weak relative to that of the heterodimerization of VDR with RXR (Fig. 4A).

Because the truncated Smad3 mutants lacking interaction with VDR suppressed the ligand-induced transactivation of VDR, it appears that the MH2 domain of Smad3 and VDR may competitively recruit the same factors. Therefore, we used nuclear extracts of cells (*26*) overexpressing FLAG-Smad3 to test for interaction with GST-VDR. FLAG-Smad3 in the nuclear extracts showed ligand-dependency in the interaction with VDR in vitro (Fig. 4B), as seen in vivo, and the MH1 region was also required for this in vitro ligand dependency (*13*). Thus, an unidentified nuclear component may stabilize the ligand-dependent complex formation of VDR with Smad3. Such components might include coactivators for VDR such as the members of the SRC-1/TIF2 protein family, which directly interact with the minimal activation domain (AD) of AF-2 in the COOH-terminal end of the E domain in a ligand-dependent manner (*3, 25, 27*). To test this possibility, we chose SRC-1, because this coactivator binds to the AF-2 AD of VDR (*25, 28*). Overexpression of SRC-1 enhanced the ligand-dependent interaction between Smad3 and VDR (Fig. 4B). The SRC-1–stabilized interaction of VDR with Smad3 was further confirmed by coimmunoprecipitation experiments (Fig. 4C) and the mammalian two-hybrid system (*13*). When VDR was either truncated [VDR(1-357)] or mutated [VDR(L417S) and VDR(E420Q)] in the AF-2 AD such that they did not interact with SRC-1 (*25*) but still interacted with Smad3 in vitro, the ligand-

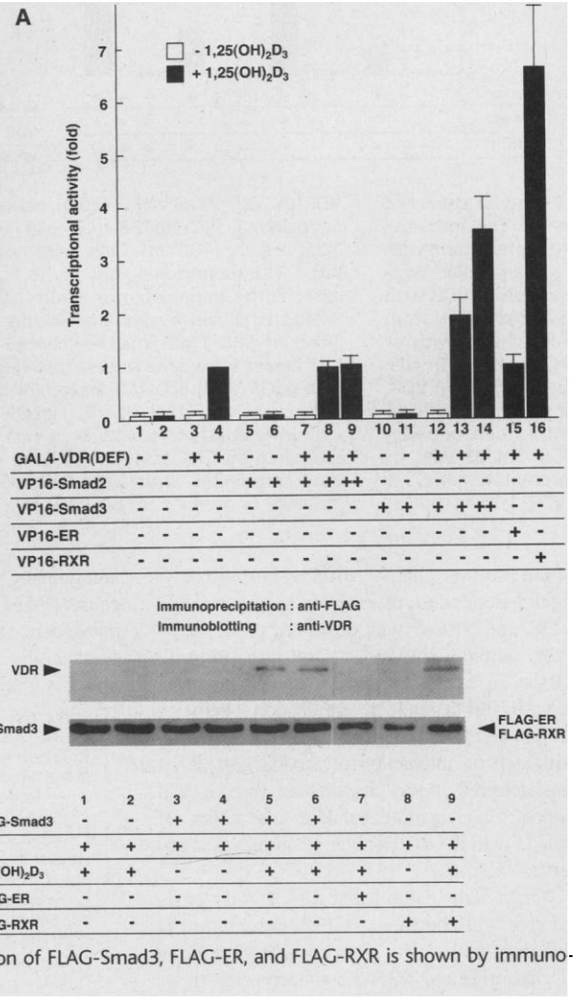

Fig. 2. Ligand-dependent interaction of Smad3 with VDR in vivo. (**A**) Interactions of SMADs with VDR were examined in the mammalian two-hybrid system in the presence (solid columns) or absence (open columns) of $1,25(OH)_2D_3$ (10^{-9} M). CAT assays were done as described (Fig. 1). COS-1 cells were transfected with CAT reporter plasmid (3 μg) bearing the GAL4-binding element (17M5-CAT), expression vector containing the DEF domain of VDR fused to GAL4 DNA-binding domain [GAL4-VDR(DEF)] (5 μg), and the expression vector [5 (+) or 10 (++) μg] bearing Smad2, Smad3, ER, or RXR fused to VP16 activation domain (VP16-Smad2, VP16-Smad3, VP16-ER, or VP16-RXR). (**B**) Coimmunoprecipitation of Smad3 and VDR. Smad3-VDR interaction was analyzed by immunoprecipitation with antibody to FLAG followed by immunoblotting using antibody to VDR. COS-1 cells were cotransfected with pSG5-VDR, pcDNA3-FLAG-Smad3, pcDNA3-FLAG-ER, or pcDNA3-FLAG-RXR (10 μg) in the presence or absence of $1,25(OH)_2D_3$ (10^{-9} M). Cells were lysed in TNE buffer, immunoprecipitated with monoclonal antibody to FLAG, and interacting proteins were detected by immunoblotting with antibody to VDR (*6*). Expression of FLAG-Smad3, FLAG-ER, and FLAG-RXR is shown by immunoblotting with antibody to FLAG.

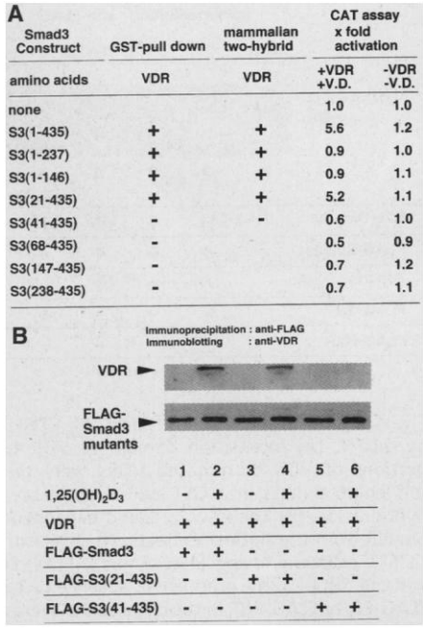

Fig. 3. Smad3 domain required for interaction with VDR. (**A**) Interaction domain of Smad3 for VDR. VDR was tested for the interaction with the indicated portions of Smad3 in a GST–pull down assay and a mammalian two-hybrid assay (–, no interaction; +, interaction; no symbol, not determined). The effects of Smad3 mutants on transactivation function of VDR were estimated by CAT assays, using the extracts from COS-1 cells expressing VDR and the truncated Smad3 mutants in the presence of $1,25(OH)_2D_3$; the fold activations by Smad3 proteins are in the right panel. (**B**) Coimmunoprecipitation of Smad3 deletion mutants and VDR. Interactions between Smad3 deletion mutants [S3(21-435) and S3(41-435)] and VDR were analyzed by immunoprecipitation with anti-FLAG followed by immunoblotting using antibody to VDR (Fig. 2). COS-1 cells were transfected with pSG5-VDR, pcDNA3-FLAG-Smad3, pcDNA3-FLAG-S3(21-435), or pcDNA3-FLAG-S3(41-434) (10 μg) in the presence or absence of $1,25(OH)_2D_3$ (10^{-9} M). Expression of FLAG-Smad3 and its mutants is shown by immunoblotting with antibody to FLAG.

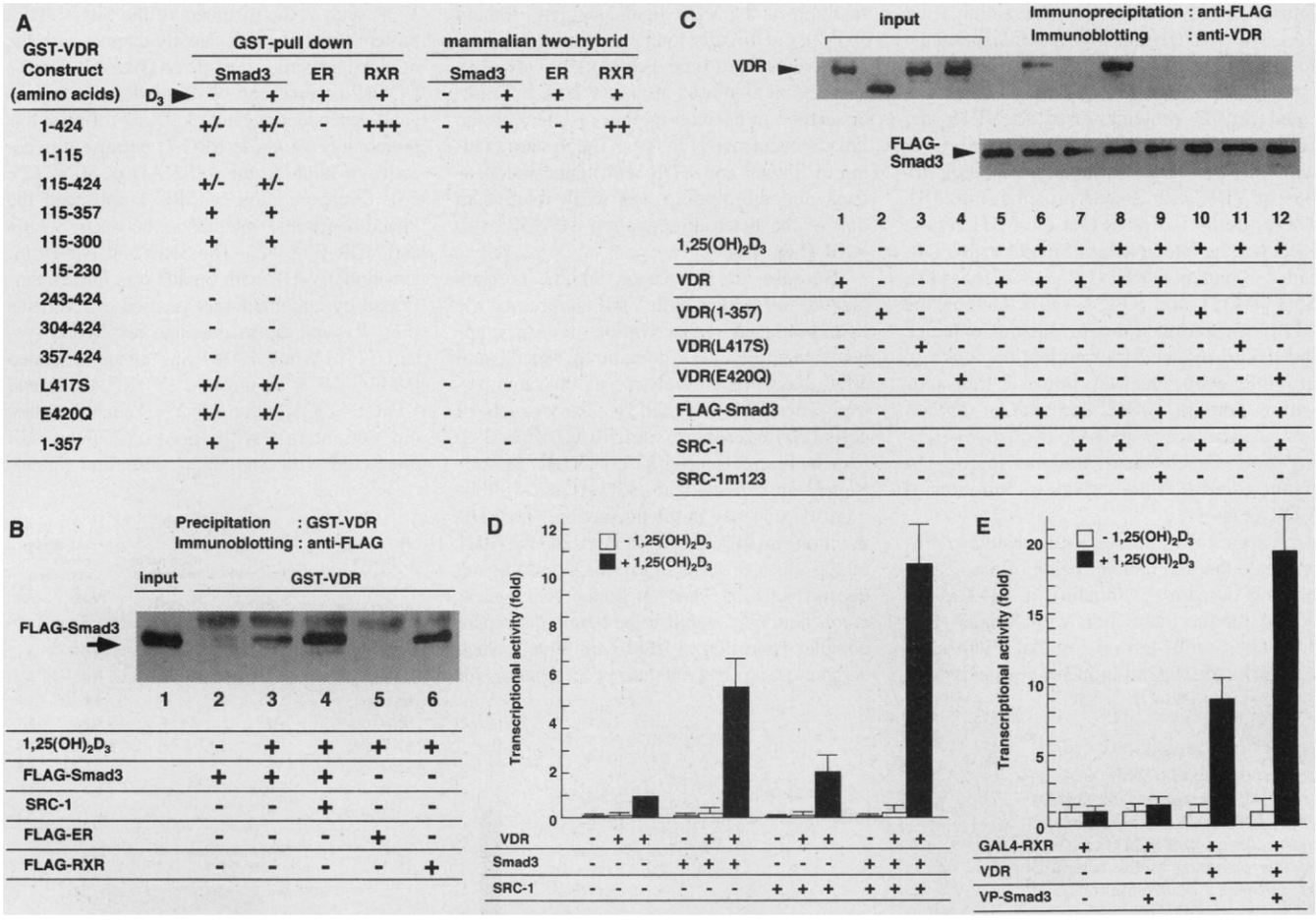

Fig. 4. Ligand-dependent formation of a VDR-Smad3 complex enhanced by SRC-1. (**A**) Interaction domain of VDR for Smad3. The indicated portions of VDR or mutated VDRs were tested for interaction with full-length Smad3 in a GST–pull down assay and a mammalian two-hybrid assay. (**B**) The in vitro ligand-dependent interaction of VDR with Smad3 from the nuclear extracts. Nuclear extracts were prepared from COS-1 cells expressing FLAG-Smad3, FLAG-ER, or FLAG-RXR with or without SRC-1 in the presence or absence of $1,25(OH)_2D_3$. FLAG-Smad3, FLAG-ER, or FLAG-RXR in the cell extracts were precipitated by GST-VDR. Interacting proteins were detected by immunoblotting with monoclonal antibody to FLAG. (**C**) Effects of SRC-1 on the interaction between Smad3 and VDR or mutated VDRs. Interactions of Smad3-VDR or Smad3-VDR mutants were analyzed by coimmunoprecipitation. COS-1 cells were cotransfected with pSG5-VDR, pSG5-VDR(1-357), pSG5-VDR(L417S), pSG5-VDR(E420Q), pcDNA3-FLAG-Smad3, pcDNA3-SRC-1, or pcDNA3-SRC-1m123 (10 μg) in the presence or absence of $1,25(OH)_2D_3$ (10^{-9} M). Cells were lysed in TNE buffer, immunoprecipitated with monoclonal antibody to FLAG, and interacting proteins were detected by immunoblotting with antibody to VDR (*6*). Expression of Smad3 is shown by immunoblotting with the antibody to FLAG. (**D**) Effect of SRC-1 on Smad3-enhanced transactivation function of VDR. CAT assays were done as described (Fig. 1). COS-1 cells were transfected with pSG5-VDR, pcDNA3-Smad3, or pcDNA3-SRC-1 in the presence or absence of $1,25(OH)_2D_3$. (**E**) Ligand-dependent interaction of Smad3 with RXR/VDR heterocomplex in vivo. Mammalian three-hybrid system estimated by CAT assays were done as described (Fig. 1). COS-1 cells were transfected with GAL4-RXR, pSG5-VDR, or VP16-Smad3 in the presence or absence of $1,25(OH)_2D_3$.

dependent interaction of VDR with Smad3 was abolished (Fig. 4C) [mutation $Leu^{417} \rightarrow Ser^{417}$ indicated as L417S (*29*)]. Conversely, overexpression of a SRC-1 mutant protein (SRC-1m123), which has point mutations in all of the three LXXLL motifs (*29*) and does not interact with VDR, inhibited the ligand-dependent interaction between Smad3 and VDR (Fig. 4C). Similar results were obtained in these assays when the TIF2 (*28*) were used instead of SRC-1 (*13*). SRC-1 augmented the Smad3-enhanced transactivation function of VDR (Fig. 4D). Thus, the ligand-dependent interaction of VDR with Smad3 apparently requires at least a member of the SRC-1/TIF2 protein family. We examined whether Smad3 binds SRC-1 directly in vitro. A ligand-dependent interaction between GST-VDR and SRC-1 was observed (*13*). However, Smad3 showed no interaction with SRC-1 or TIF2 (*13*). Finally, we confirmed the ligand-dependent interaction between Smad3 and RXR/VDR heterocomplex in vivo. Although no interaction of Smad3 with RXR was detected in the mammalian three-hybrid system, the ligand-dependent interaction of Smad3 with RXR/VDR heterocomplex was observed (Fig. 4E).

Our results established a molecular basis for cross-talk between TGF-β and vitamin D signaling pathways. The cooperative actions of vitamin D and TGF-β can be synergistic or antagonistic in a tissue-specific manner. Because SMAD proteins are differentially expressed in target tissues for TGF-β, the tissue-specific amounts of endogenous SMAD proteins may contribute to the cooperative actions.

References and Notes

1. D. J. Mangelsdorf *et al.*, *Cell* **83**, 835 (1995).
2. A. W. Norman, J. Roth, L. Orchi, *Endocr. Rev.* **3**, 331 (1982); H. F. DeLuca, *Adv. Exp. Med. Biol.* **196**, 361 (1986); M. R. Walters, *Endocr. Rev.* **13**, 719 (1992); M. R. Hausller *et al.*, *J. Bone Miner. Res.* **13**, 325 (1998).
3. S. A. Onate *et al.*, *Science* **270**, 1354 (1995); E. Kalkhoven *et al.*, *EMBO J.* **17**, 232 (1998); H. Chen *et al.*, *Cell* **90**, 569 (1997); J. Torchia *et al.*, *Nature* **387**, 677 (1997); K. B. Horwitz *et al.*, *Mol. Endocrinol.* **10**, 1167 (1996); J.-M. Wurtz *et al.*, *Nature Struct. Biol.* **3**, 87 (1996).

4. Y. Kamei *et al.*, *Cell* **85**, 403 (1997); D. Chakravarti *et al.*, *Nature* **383**, 99 (1996); H. Kawasaki *et al.*, *ibid.* **393**, 284 (1998).
5. P. H. Stern, in *Vitamin D*, D. Feldman, F. H. Glorieux, J. W. Pike, Eds. (Academic Press, New York, 1997), pp. 343–345; A. Takeshita *et al.*, *J. Biol. Chem.* **273**, 14738 (1998).
6. T. Yoshizawa *et al.*, *Nature Genet.* **16**, 391 (1997).
7. S. Kato *et al.*, *Science* **270**, 1491 (1995); K. Takeyama *et al.*, *ibid.* **277**, 1827 (1997).
8. K. Ebihara *et al.*, *Mol. Cell. Biol.* **16**, 3393 (1996).
9. S. Kato *et al.*, *ibid.* **15**, 5858 (1995).
10. COS-1 cells were maintained in Dulbecco's modified Eagle's medium without phenol red, supplemented with fetal bovine serum (5%) treated with dextran-coated charcoal. The cells were transfected at 40 to 50% confluency in 10-cm petri dishes with a total of 20 μg of the indicated plasmids using calcium phosphate. All assays were done in the presence of 3 μg of pCH110 (Pharmacia), a β-galactosidase expression vector, as an internal control to normalize for variations in transfection efficiency. Cognate ligands were added to the medium 1 hour after transfection and at each exchange of medium. After 24-hour incubation with the calcium phosphate–precipitated DNA, the cells were washed with fresh medium and incubated for an additional 24 hours. Cell extracts were prepared by freezing and thawing and were assayed for CAT activity after normalization for β-galactosidase activity as described (*9*).
11. The mammalian expression vector pcDNA3 (Invitrogen) was used for the expressions of Smad and SRC-1 proteins. Constitutively active and catalytically inactive forms of TβR-I, BMPR-IA, and BMPR-IB were as described (*12*). Full-length VDR and VDR mutants were inserted into the mammalian expression vector pSG5 (pSG5-VDR). DEF domains of VDR were inserted into the pM vector (Clontech) [GAL4-VDR(DEF)] and full-length Smad2 and Smad3 were inserted into pVP (Clontech) (VP16-Smad2 and VP16-Smad3).
12. T. Imamura *et al.*, *Nature* **389**, 622 (1997).
13. J. Yanagisawa *et al.*, unpublished data.
14. J. Massague, *Cell* **85**, 947 (1996); C.-H. Heldin, K. Miyazono, P. ten Dijke, *Nature* **390**, 465 (1997); J. R. Howe *et al.*, *Science* **280**, 1086 (1998).
15. M. Kretzschmar *et al.*, *Genes Dev.* **11**, 984 (1997); A. Suzuki *et al.*, *Dev. Biol.* **184**, 402 (1997); J. M. Graff, A. Bansal, D. A. Melton, *Cell* **85**, 479 (1996).
16. P. A. Hoodless *et al.*, *Cell* **85**, 489 (1996); F. Liu *et al.*, *Nature* **381**, 620 (1996).
17. M. Macias-Silva *et al.*, *Cell* **87**, 1215 (1996); A. Nakao *et al.*, *EMBO J.* **16**, 5353 (1997); J. C. Baker and R. M. Harland, *Genes Dev.* **10**, 1880 (1996).
18. G. Lagna *et al.*, *Nature* **383**, 832 (1996); Y. Zhang *et al.*, *ibid.*, p. 168.
19. X. Chen, M. J. Rubock, M. Whitman, *ibid.*, p. 691; J. Kim *et al.*, *ibid.* **388**, 304 (1997); S. Dennler *et al.*, *EMBO J.* **17**, 3091 (1998); L. Zawel *et al.*, *Mol. Cell* **1**, 611 (1998).
20. Y. Zhang, T. Musci, R. Derynck, *Curr. Biol.* **7**, 270 (1997).
21. GAL4 DNA-binding domain fusions were generated in pM, and VP16 fusions within pVP16. Interactions were tested in COS-1 cells. Activation of the CAT reporter–bearing GAL4-binding elements (17Mx5) was assayed in the presence or absence of $1,25(OH)_2D_3$.
22. COS-1 cells were transfected with the indicated plasmids, lysed in TNE buffer [10 mM Tris-HCl (pH 7.8), 1% NP-40, 0.15 M NaCl, 1 mM EDTA], and immunoprecipitated with monoclonal antibody to FLAG (IBI; Eastman Kodak). Interacting proteins were separated by 8% SDS–polyacrylamide gel electrophoresis (SDS-PAGE), transferred onto polyvinylidene difluoride membranes (Bio-Rad), and then detected with antibody to VDR and antibody to rabbit immunoglobulin G conjugated with alkaline phosphatase (Promega).
23. GST-fused proteins were expressed in *Escherichia coli* and purified on glutathione-Sepharose beads (Pharmacia). The beads were incubated with [^{35}S]methionine-labeled proteins. Bound proteins were eluted and analyzed by SDS-PAGE.
24. Proteins were translated in vitro in the presence of [^{35}S]methionine with the reticulocyte lysate system (Promega).
25. D. M. Heery *et al.*, *Nature* **387**, 733 (1997); H. Masuyama *et al.*, *Mol. Endocrinol.* **11**, 1507 (1997); C. H. Jin *et al.*, *ibid.* **10**, 945 (1996).
26. Cells were harvested and washed twice with ice-cold phosphate-buffered saline. Centrifuged cells were resuspended in 4 ml ice-cold lysis buffer [10 mM Tris-HCl (pH 7.4), 10 mM NaCl, 3 mM $MgCl_2$, 0.5% (v/v) NP-40] and incubated on ice for 15 min, then centrifuged again for 5 min at 500*g*. The sedimented nuclear fraction was resuspended in TNE buffer [10 mM tris-HCl (pH 7.8), 1% NP-40, 0.15 M NaCl, 1 mM EDTA], incubated for 30 min on ice, and centrifuged. The supernatant was used as nuclear extract for the experiments.
27. T. Spencer *et al.*, *Nature* **389**, 194 (1997); T. Yao *et al.*, *Proc. Natl. Acad. Sci. U.S.A.* **93**, 10626 (1997).
28. J. J. Voegel *et al.*, *EMBO J.* **17**, 507 (1998).
29. Single-letter abbreviations for the amino acid residues are as follows: A, Ala; C, Cys; D, Asp; E, Glu; F, Phe; G, Gly; H, His; I, Ile; K, Lys; L, Leu; M, Met; N, Asn; P, Pro; Q, Gln; R, Arg; S, Ser; T, Thr; V, Val; W, Trp; and Y, Tyr. X indicates any residue.

30. We thank P. Chambon for critical reading of the manuscript and for providing nuclear receptor expression vectors, H. Gronemeyer for providing TIF2 expression vectors, R. H. Goodman for the CBP cDNA, and S. Hanazawa and A. Takeshita for helpful discussion.

23 June 1998; accepted 22 January 1999

p53- and ATM-Dependent Apoptosis Induced by Telomeres Lacking TRF2

Jan Karlseder,[1]* Dominique Broccoli,[1]*† Yumin Dai,[2] Stephen Hardy,[2]‡ Titia de Lange[1]§

Although broken chromosomes can induce apoptosis, natural chromosome ends (telomeres) do not trigger this response. It is shown that this suppression of apoptosis involves the telomeric-repeat binding factor 2 (TRF2). Inhibition of TRF2 resulted in apoptosis in a subset of mammalian cell types. The response was mediated by p53 and the ATM (ataxia telangiectasia mutated) kinase, consistent with activation of a DNA damage checkpoint. Apoptosis was not due to rupture of dicentric chromosomes formed by end-to-end fusion, indicating that telomeres lacking TRF2 directly signal apoptosis, possibly because they resemble damaged DNA. Thus, in some cells, telomere shortening may signal cell death rather than senescence.

Mammalian telomeres consist of several kilobases of tandem TTAGGG repeats bound by the related telomere-specific proteins, TRF1 and TRF2 (*1*). TRF1 regulates telomere length (*2*) and TRF2 maintains telomere integrity (*3*). Inhibition of TRF2 results in loss of the G-strand overhangs from telomere termini and induces covalent fusion of chromosome ends (*3, 4*).

To investigate the cellular consequences of telomere malfunction, we used adenoviral vectors to overexpress intact and truncated versions of TRF1 and TRF2 (Fig. 1) (*5*). These vectors encoded full-length TRF1 (AdTRF1); a dominant negative version of TRF1 lacking the Myb DNA binding domain (AdTRF1$^{\Delta M}$); full-length TRF2 (AdTRF2); an NH_2-terminal deletion of TRF2 lacking the TRF2-specific basic

Table 1. Cell type dependence of AdTRF2$^{\Delta B\Delta M}$-induced apoptosis.

Cell line/strain	Chromosome fusions per anaphase*		% cells undergoing apoptosis†	
	Uninfected	AdTRF2$^{\Delta B\Delta M}$	Uninfected	AdTRF2$^{\Delta B\Delta M}$
HeLaII‡ (cervical carcinoma)	0.1 ± 0.01	1.2 ± 0.04	2.7 ± 0.6	38 ± 1.0
HeLa1.2.11‡ (cervical carcinoma)	0.1 ± 0.01	0.9 ± 0.07	2.0 ± 1.0	40 ± 1.7
MCF7 (mammary adenocarcinoma)	0.1 ± 0.01	0.9 ± 0.06	3.0 ± 1.0	29 ± 1.2
CD4$^+$ T cells	0.2 ± 0.01	0.9 ± 0.02	6.3 ± 0.6	39 ± 1.5
HT-1080 (fibrosarcoma)	0.1 ± 0.01	0.9 ± 0.03	1.0 ± 0.1	1.3 ± 0.6
Saos-2 (osteosarcoma)	<0.1	1.3 ± 0.01	2.0 ± 1.0	2.3 ± 0.6
SW 626 (ovarian carcinoma)	<0.1	0.9 ± 0.04	3.0 ± 0.1	3.7 ± 0.6
WI-38 (fetal lung fibroblasts)	<0.1	1.2 ± 0.01	<0.01	<0.01
HS68 (foreskin fibroblasts)	<0.1	0.9 ± 0.10	<0.01	<0.01
MRC-5 (fetal lung fibroblasts)	<0.1	0.9 ± 0.08	<0.01	<0.01
IMR-90 (fetal lung fibroblasts)	<0.1	1.5 ± 0.01	<0.01	<0.01

*Infected cells (72 hours) were stained with DAPI and anaphases were examined for evidence of chromosome fusions (chromatin bridges and lagging chromosomes). The numbers indicated average fusion events per anaphase from three independent experiments and the SD. SDs below 0.01 are given as 0.01. †Percentage of cells positive for TUNEL labeling 72 hours after infection. Apoptotic CD4$^+$ T cells were counted 48 hours after infection. The numbers are averages from three independent experiments and the SD. SDs below 0.1 are given as 0.1. ‡HeLaII and HeLa1.2.11 are HeLa subclones.